UNIVERSITY OF TWENTE.

Faculty of Science & Technology,
MSc Biomedical Engineering

Source Reconstruction and Parameter Estimation of Generalized Periodic Discharges

Thomas Slingerland
M.Sc. Thesis
July 2023

Supervisors:
prof dr. ir. Michel J.A.M. van Putten
dr. ir. Arjan Hillebrand
dr. Prejaas K.B. Tewarie

Clinical Neurophysiology Group
Faculty of Science & Technology
University of Twente

Acknowledgments

Looking back on the process of my master's assignment I can truly say that I am proud of what I have accomplished. I have learned a lot, both on a professional and personal level. I have developed new technical skills, improved my writing skills and came to understand my way of working effectively. I thoroughly enjoyed the discussions with my supervisors and felt welcome in the Clinical Neurophysiology Group. I would like to acknowledge those who contributed.

First, I would like to thank my daily supervisor, Prejaas Tewarie. His enthusiasm about my masters assignment kept me enthusiastic as well and motivated to give this assignment my all. Our weekly discussions were enervating and he was a great sparring partner. When I got stuck he was able to point me into a new direction or we were able solve the issue together. Next, I would like to thank Arjan Hillebrand, my external supervisor, for his sharp comments and enthusiasm about the assignment. He has helped me greatly in creating an accurate source reconstruction pipeline and was always available to discuss the topic when I had questions. I also would like to thank Michel van Putten. His outside look on the project, especially on source reconstruction, really pushed me into being very critical and thorough when explaining the results. It was very enervating discussing the masters assignment with him and I also enjoyed playing music together.

Moreover, I want to thank Rianne for celebrating my highs with me and giving me a mental boosts when I hit a low. It was helpful that I could just walk out into the Technohal and have a quick chat to get me on my feet or share my joy about the assignment. Lastly, I want to thank 'stelletje 9 studenten' for providing distraction from my masters assignment by dragging me away to take breaks and playing cards. I hope that I can prove the name or set an example for all of you guys to try and beat.

Source reconstruction and parameter estimation of generalized periodic discharges

Thomas Slingerland[1], Michel J.A.M. van Putten[1], Arjan Hillebrand[2], Prejaas K.B. Tewarie[1,2],
[1]Clinical Neurophysiology, Institute for Technical Medicine, University of Twente, Technical Medical Centre, Enschede, The Netherlands; [2] Department of Neurology, Clinical Neurophysiology and MEG Center, Amsterdam Neuroscience, Vrije Universiteit Amsterdam, Amsterdam UMC, Amsterdam, The Netherlands.

***Abstract*- Generalized Periodic Discharges (GPDs) occur in 20% of postanoxic comatose patients. The underlying pathophysiology of GPDs is far from understood. In a previous study, a cortical meanfield model has been used to explain the pathophysiology of GPDs. In another study, source reconstruction revealed that GPDs originate in subcortical structures, mainly the thalamus. However in both cases, no distinction was made between GPDs on a continuous background and GPDs on a suppressed background. GPDs on a continuous background are associated with a good outcome, whilst GPDs on a suppressed background are associated with a poor outcome. Why this difference in outcome occurs remains unclear. In this study, we used source reconstruction, and parameter estimation on a corticothalamic meanfield model to investigate whether a difference in anatomical source and / or pathophysiological mechanisms could explain the difference in outcome between the two types of GPDs, and in the process elucidate the underlying pathophysiology of GPDs.**

From an existing dataset of continuous electroencephalograms (EEGs) of 47 patients with GPDs, we identified 26 patients with GPDs on a continuous background and 19 patients with GPDs on a suppressed background. We also included 50 EEGs from healthy controls for the estimation of reference values for the parameters of the corticothalamic meanfield model.

Source reconstruction results revealed that the anatomical source of both types of GPDs was located predominantly in the subcortical regions. We found no significant difference between the two types of GPDs. Parameter estimation revealed significant differences in the cortical and corticothalamic loop variables between both GPD groups and healthy controls. Both GPD groups exhibited significantly lower cortical loop values and predominantly negative corticothalamic loop values compared to mostly positive values in healthy controls. The corticothalamic delay was also significantly higher in the GPD groups. There were no significant differences between the two types of GPDs, except for the decay rate.

We concluded that the difference in prognosis between the two types of GPDs could not be explained by a difference in anatomical source or pathophysiological variables of the corticothalamic meanfield model, despite the significant difference in decay rate. We hypothesize that the difference in prognosis could be attributed to the continuous background, yet further research is needed. Next, our results indicate that both the cortical and corticothalamic loop are involved in the spread or generation of GPDs. In both cases the strength of the inhibitory neurons increased relative to the strength of the excitatory neurons.

***Index Terms*- Generalized Periodic Discharges, Postanoxic Encephalopathy, Source Reconstruction, Parameter Estimation, Electroencephalography**

1. Introduction

Coma as a result of postanoxic encephalopathy occurs in 75% of all survivors of out-of-hospital cardiac arrest. The mortality rate in these patients is 50%, making postanoxic encephalopathy the most important cause of death in the hospital [1]. Electroencephalography (EEG) is used for the prognosis of the neurological outcome in these comatose patients [2]. Specific EEG patterns are associated with a poor prognosis that are indicative of severe brain damage, and the patient is likely not to survive or will be severely disabled. Some examples of these patterns are burst suppression, generalized suppression, and generalized periodic discharges (GPDs) on a suppressed background [3, 4, 5].

Generalized periodic discharges are defined in the latest guideline on standardized EEG terminology by the American Clinical Neurophysiology Society [6] as: "any bilaterally synchronous and symmetric repetition of a waveform with relatively uniform morphology and duration with a clearly discernible interdischarge interval between consecutive waveforms and recurrence of the waveform at nearly regular intervals." These waveforms are characterized by a duration of 0.5 s or less or limited to 3 phases. Although there is a clear definition of what

can be considered as a GPD, there is still little understanding as to where in the brain these GPDs originate or what the underlying pathophysiology is.

An explanation of the underlying pathophysiology has been proposed in [7]. They used a meanfield model of the cortex and suggested that GPDs are generated due to a disruption of the balance between the excitatory and inhibitory inputs of pyramid cells, resulting in a disinhibition of excitatory pyramid cells. This disruption is caused by anoxia due to cardiac arrest, creating metabolic derangements that, in turn, disrupt synaptic transmissions. Synaptic transmissions of excitatory pyramidal cells and inhibitory interneurons are especially affected due to their relative sensitivity to hypoxia. Their choice of a cortical meanfield model was based on the assumption that GPDs originate in the cortex. A later paper discovered, using EEG source reconstruction, that the thalamus, hippocampus, and amygdala are likely the source from which GPDs originate [3]. This result motivates to investigate the underlying pathophysiology of GPDs using a corticothalamic meanfield model.

Both research studies [3, 7] do not differentiate between GPDs on a suppressed or continuous background. However, a paper by Ruijter et al. [5] showed that there is a difference in recovery from postanoxic encephalopathy between patients with GPDs on a continuous background and patients with GPDs on a suppressed background. In this study, none of the patients who developed GPDs on a suppressed background (38% of the study population) survived. However, all patients who recovered with a Cerebral Performance Category (CPC) of 1-2, considered a complete recovery or recovery with mild cerebral dysfunction, had a continuous background prior to the occurrence of GPDs (10% of the study population). They concluded that GPDs on a suppressed background are associated with a poor outcome (CPC 3-5), which corresponds to severe cerebral dysfunction, vegetative state, or death, and patients who experience GPDs on a continuous background have a greater chance of a good outcome (CPC 1-2). The difference in outcome between patients with GPDs on a suppressed background and patients with GPDs on a continuous background could suggest a difference in the underlying pathophysiology and / or in the anatomical source of both types of GPDs.

In this paper, we investigated the anatomical source and underlying pathophysiology of GPDs on a suppressed background and of GPDs on a continuous background, by means of EEG source reconstruction, and parameter estimation on a corticothalamic meanfield model. Based on previous research, we hypothesized that for both types of GPDs the anatomical source lies in the subcortical regions: around the thalamus, hippocampus, and amygdala. Our objective was to identify whether the difference in prognosis between the two types of GPD could be explained by a difference in anatomical source and / or pathophysiological mechanisms, and in the process, elucidate the underlying pathophysiology of GPDs.

2. Background

In this section, we describe the pathophysiology of postanoxic encephalopathy. Additionally, we provide a more detailed description of the methods used in this thesis. This includes explaining the mathematical principles underlying source reconstruction and parameter estimation, as well as providing a substantiation for our choice of inverse solution.

2.1. Postanoxic Encephalopathy

Postanoxic encephalopathy refers to an altered brain function and / or structure (encephalopathy) due to a lack of oxygen (anoxia) [8]. In our case, cardiac arrest causes the anoxia and encephalopathy is presented as a comatose state. After resuscitation, the eventual outcome of comatose patients (or the extent of their encephalopathy) is characterized by the transition from reversible to irreversible brain damage. This transition occurs in minutes, hours or days depending on the level of the remaining blood flow, duration of the ischaemia, and the extent of reperfusion [9]. The paragraphs below describe this transition in more detail and are primarily based on the research conducted in [9] supported by additional sources.

The brain contributes only 2% to the total body weight, yet it is responsible for 20% of the total body oxygen consumption and 25% of the total body glucose utilization [10]. This high metabolism, in combination with the lack of any glucose reserves, makes it highly susceptible to any blood flow interruption. Insufficient blood flow (ischaemia) and oxygen delivery (hypoxia) results in loss of neuronal function within 60 seconds [11]. On this time scale, loss of neuronal function is reversible, however if the ischaemia persists for merely minutes, the brain could be irreversibly damaged [12].

In the first minute of ischaemia, synaptic activity disappears as a result of synaptic failure [13]. Lack of oxygen and steady depletion of glucose levels starts to impair the release of presynaptic neurotransmitters [14]. In turn, this inhibits propagation of action potentials between neurons. A persistence of synaptic failure leads, after a few minutes, to massive cortical synaptic failure which is reflected in a suppressed EEG pattern. If the suppressed EEG pattern persists over 6-24 hours it is associated with transitions towards permanent brain damage [15].

Depending on the remaining perfusion levels, within minutes to a few hours, cerebral glucose and ATP stores are depleted [10]. This results in the dysfunction of ATP-depended ion pumps, especially sodium-potassium pumps. The dysfunction of the pumps leads to the loss of ion gradients across the plasma membrane, which causes the inability to generate action potentials [10]. Furthermore, the loss of ion gradients causes a net flow of

ions to the intracellular space. This increase in osmolality causing an inflow of water leading to cell swelling [16]. In the early stages, this can be reversed by reperfusion. In the absence of reperfusion, necrotic cell death will occur.

ATP-dependent calcium channels also start to dysfunction due to lack of cerebral glucose, causing an influx of calcium into the intracellular space [10]. In a time span of up to 72 hours, the increase of calcium levels in the intracellular space leads to the release of cytochrome C and mediates the release of glutamate, both cause a cascade leading towards apoptosis [17, 18].

Even the reperfusion may cause additional brain damage. Reperfusion is often unevenly distributed due to vasospasms, increased blood viscosity and platelett aggregation causing local hypoperfusion [19]. Furthermore, it causes an inflamma-
tory response and microvascular damage, and radical and reactive oxygen species present may cause lipid and protein degradation [10].

Based on the paragraphs above, the transition from reversible to irreversible damage lies between hours to days. The longer it takes for reperfusion to occur, the greater the chance of irreversible brain damage. The largest opportunity to reverse the damage is in the first few hours.

2.2. Source Reconstruction

Source reconstruction is a technique "to model and estimate the spatiotemporal dynamics of neuronal currents throughout the brain that generate the electric potentials and magnetic fields measured with noninvasive or invasive electromagnetic recording technologies [20]." Source reconstruction has three parts: a forward solution which includes the anatomical information, the functional data, and the inverse solution (figure 1).

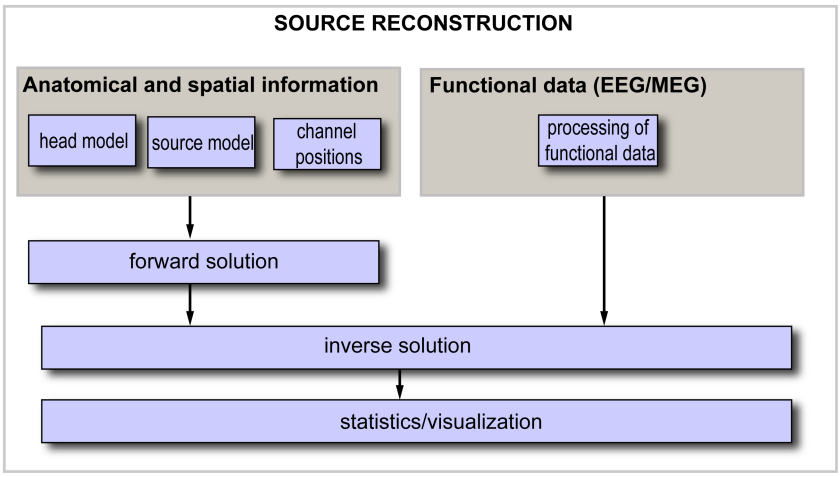

Figure 1: Schematic diagram of source reconstruction [21].

The forward solution determines how much a given electrical source in the brain will influence the potential on each electrode on the scalp [22]. The impact of all electrical sources on each electrode in the scalp is captured in a leadfield matrix. To create a leadfield matrix you need: a description of the geometrical and conductivity properties of the head (a headmodel), a set of electrical point sources spread out in a source space (a source model), and the positions of the scalp electrodes [20, 22].

The inverse solution uses the leadfield matrix and EEG data to give an approximation of the source location of the electrical potentials measured with the EEG [20]. In this thesis we chose eLORETA (exact low resolution brain electromagnetic tomography) for the inverse solution. A justification of this choice is provided later in this section. eLORETA is an inverse solution which provides exact, zero error localization in the presence of measurement and biological noise (mathematical proof is presented in [23]) and uses depth weighting to focus on deep sources in the brain [23, 24]. It translates mathematically to

$$\hat{j}_i = W_i^{-1} K_i^T (K W^{-1} K^T + \alpha H)^+ \Phi \tag{1}$$

in which: $\hat{j}$ is the current density at voxel i (in Am^2), W is the weight matrix, K the leadfield matrix, Φ the EEG data, α the regularization parameter, H the average reference operator, and $^+$ denotes a Moore-Penrose inverse. α factors in EEG noise and enforces a level of smoothness [22]. H makes sure that any inverse solution will not depend on the reference electrode [23]. Simplified, the current density is obtained by a multiplication of the leadfields and the EEG data, in which the current density over all voxels reveals the source activity. Peaks in the source activity reveal the source location(s).

2.2.1. Choice for eLORETA

There are many ways to calculate the inverse solution [25]. The choice of eLORETA was based on a few assumptions. First, it was assumed that GPDs could have multiple sources. This eliminates the use of dipole fitting and beamformers, because they are mainly used to localise one source. Second, the source was expected to be present in the subcortical structures. Third, we decided to use the Fieldtrip toolbox due to its MATLAB compatibility and extensive amount of tutorials [21]. The first assumption limits the inverse solutions to those based on minimum norm estimation. The second assumption brings us to the LORETA (low resolution brain electromagnetic tomography) or LAURA (local auto-regressive average) inverse solution. Both of these methods outperformed other methods in depth resolution [26, 27, 28]. However, due to the third assumption we could not use LAURA or LORETA. FieldTrip does however include eLORETA and sLORETA (standardized low resolution brain electromagnetic tomography). Both inverse solutions are also capable of detecting deep sources, with eLORETA outperforming sLORETA in depth resolution [24, 28].

2.2.2. Sensitivity

The feasibility of detecting subcortical signals with EEG is up for debate [29]. It is therefore a valid concern whether the sensitivity of source reconstruction is adequate enough to detect subcortical sources based on these signals. In this section, we want to address this concern by providing literary proof that source reconstruction is sensitive enough to resolve subcortical sources.

Strong evidence that subcortical signals can be sensed by a scalp EEG, and therefore can be used to reconstruct subcortical activity, is provided in [29]. They measured high-density scalp EEG simultaneously with intracranial electrodes in the central medial thalamus and nucleus accumbens in DBS-patients. During the measurements, the patients were in rest with their eyes closed. They found a significant correlation between the alpha envelopes derived from intracranial electrodes and EEG source reconstructed signals. For the source reconstruction they used a Locally Spherical Model with Anatomical Constraints (LSMAC) as a headmodel and LAURA for the inverse solution. The highest correlation was found for source signals in close proximity to the actual recording sites, given by the DBS electrode locations. This provides direct evidence that scalp EEG can sense subcortical signals and that these signals are contributed to the correct source. Other studies support the claim that subcortical signals can be correctly reconstructed by means of source reconstruction [30, 31].

In [29] they used high-density EEG to prove that subcortical sources can be reconstructed correctly. Our data consists of low-density EEG recordings. However, previous studies have shown that in cases of high signal to noise ratio (SNR), such as GPDs, low-density electrical source imaging is reliable enough to localise these sources [32, 33]. Furthermore, previous studies have shown that our intended method for source reconstruction, with low-density EEG recordings, can correctly identify subcortical sources [33, 34, 35].

2.3. Parameter Estimation

Parameter estimation is a method for determining the values of the parameters of a model based on measured data. In this thesis, we employed a corticothalamic meanfield model to investigate the underlying pathophysiology of GPDs. This model represents the corticothalamic system in which the parameters correspond to physiological variables in this system. We explored the parameter space of this model with the use of the Metropolis-Hastings algorithm to find the best parameter fit that explains the onset of GPDs. Both the model and the use of Metropolis-Hastings for parameter estimation are based on papers by Abeysuriya and Robinson [36, 37]. We will provide a detailed explanation of both in subsequent sections.

2.3.1. Corticothalamic meanfield model

The corticothalamic meanfield model consists of four neural populations, excitatory(e) and inhibitory (i) cortical neurons, thalamic relay neurons (s), thalamic reticular neurons (r) and an external sensory input(n), making up the corticothalamic system (figure 2).

Six equations form the mathematical corner stone of this model. These six equations describe the interdependent connections and dynamics of the four neural populations. The first equation is a sigmoid function, S, which relates the mean firing rate Q_a, of population a with spatial vector $\mathbf{r}$ and temporal vector t, to the corresponding mean soma potential V_a relative to resting

$$Q_a(\mathbf{r},t) = S(V_a(\mathbf{r},t)) = \frac{Q_{max}}{1 + exp[-(V_a(\mathbf{r},t) - \theta)/\sigma']} \tag{2}$$

In this equation Q_{max} is the maximum firing rate, θ expresses the mean threshold voltage and σ' is the standard deviation of the threshold distribution equal to $\frac{\pi}{\sqrt{3}}$.

Equation 3-5 describe the potential V_a and its dependency on the contributions of the firing rate from the presynaptic populations ϕ_b, the strength of the connections to populations a from b ν_{ab}, and the smoothing effects arising from synaptodendritic dynamics and soma capacitance $\frac{1}{\alpha}$, $\frac{1}{\beta}$, τ_{ab}. They represent respectively the decay and rise time of the response at the cell body and a time delay due to discrete anatomical separations

between the populations.

$$V_a(\mathbf{r},t) = \sum_b V_{ab}(\mathbf{r},t) \tag{3}$$

$$D_\alpha(t)V_{ab}(\mathbf{r},t) = \nu_{ab}\phi_b(\mathbf{r},t-\tau_{ab}) \tag{4}$$

$$D_\alpha = \frac{1}{\alpha\beta}\frac{d^2}{dt^2} + (\frac{1}{\alpha}+\frac{1}{\beta})\frac{d}{dt} + 1 \tag{5}$$

ν_{ab} is further defined as $\nu_{ab} = s_{ab}N_{ab}$ where N_{ab} is the mean number of synapses per neuron a from neurons of type b and s_{ab} is the mean time-integrated strength of soma response per incoming spike. $\frac{1}{\alpha}$, $\frac{1}{\beta}$ are the same for every connection between populations and only $\tau_{es} = \tau_{is} = \tau_{se} = \tau_{re} = t_0/2$ are nonzero with t_0 as the total time delay for the corticothalamic feedback loop.

The last two equations describe the propagation of the outgoing firing rate $\phi_a(\mathbf{r},t)$, with $\gamma_a^2 = v_a/r_a$ as the temporal damping rate, v_a as the propagation velocity, and r_a as the mean distance.

$$D_a(\mathbf{r},t)\phi_a(\mathbf{r},t) = Q_a \tag{6}$$

$$D_a(\mathbf{r},t) = \frac{1}{\gamma_a^2}\frac{\partial^2}{\partial t^2} + \frac{2}{\gamma_a}\frac{\partial}{\partial t} + 1 - r_a^2\nabla^2 \tag{7}$$

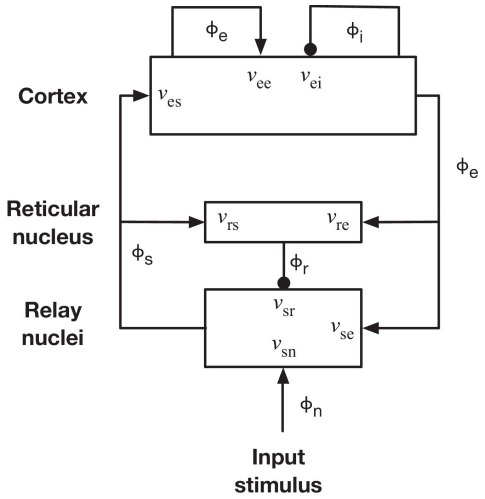

Figure 2: Schematic diagram of the corticathalamic model of Abeysuriya and Robinson [37, 36].The neural populations shown are cortical excitatory e and inhibitory i, thalamic reticular r and thalamic relay nuclei s. The parameter ν_{ab} quantifies the connection from population b to population a. Excitatory connections are shown with pointed arrowheads, and inhibitory connections are shown with with round arrowheads. ϕ_b is the firing rate.

EEG power spectrum The model outputs an EEG power spectrum based on the previous six equations. It takes the following series of steps and assumptions into account to arrive at this power spectrum.

First, equation 2 is linearized. This is based on previous work which has revealed that most brain states occur in the linear regime of the model [37, 38], with $\rho_a = S'(V_a^{(0)})$ and S' the derivative of the sigmoid function at the steady state value $V_a^{(0)}$.

$$Q_a(\mathbf{r},t) = \rho_a V_a(\mathbf{r},t) \tag{8}$$

Next, the Fourier transform is taken of equation 3-8, which results in an expression for ϕ_e in terms of ϕ_n. In this expression $G_{ab} = \rho_a\nu_{ab} = \rho_a N_{ab}S_{ab}$ is the response in neurons a to unit input from neurons b and $G_{ese} = G_{es}G_{se}$, $G_{esre} = G_{es}G_{sr}G_{re}$ and $G_{srs} = G_{sr}G_{rs}$ correspond to the overall gains of the excitatory corticothalamic, inhibitory corticothalamic and intrathalamic loops, respectively.

$$\frac{\phi_e(\mathbf{k},\omega)}{\phi_n(\mathbf{k},\omega)} = \frac{G_{es}G_{sn}L^2 exp(i\omega t_0/2)}{(1-G_{srs}L^2)(1-G_{ei}L)(k^2r_e^2+q^2r_e^2)} \tag{9}$$

$$q^2r_e^2 = \left(1-\frac{i\omega}{\gamma_e}\right)^2 - \frac{1}{1-G_{ei}L}\left\{LG_{ee} + \frac{[L^2G_{ese}+L^3G_{esre}]e^{i\omega t_0}}{1-L^2G_{srs}}\right\} \tag{10}$$

$$L(\omega) = (1-i\omega/\alpha)^{-1}(1-i\omega/\beta)^{-1} \tag{11}$$

To calculate the EEG power spectrum $P(\omega)$, $\phi_e(\mathbf{k},\omega)$ is integrated over $\mathbf{k}$, with $\mathbf{k}$ being the wave vector with magnitude $k = 2\pi/\lambda$ and the input stimulus ϕ_n is taken to be white noise. The cortex is approximated by a rectangular sheet given by L_xXL_y and $F(k)$ approximates the low-pass spatial filtering due to volume conduction of the cerebrospinal fluid, skull and scalp, which can be approximated by: $F(k) = e^{-k^2/k_0^2}$

$$P(\omega) = \sum_{m=-\infty}^{\infty} \sum_{n=-\infty}^{\infty} |\phi_e(k_x, k_y, \omega)|^2 F(k) \Delta k_x \Delta k_y \tag{12}$$

$$k_x = \frac{2\pi m}{L_x}, k_y = \frac{2\pi n}{L_y}, k = \sqrt{k_x^2 + k_y^2} \tag{13}$$

2.3.2. MCMC-MH

In this section, we will first explain the underlying principles of the Metropolis-Hastings algorithm, and then discuss its application in parameter estimation.

Monte Carlo is an algorithm which draws random samples from a target distribution to come to a probability distribution. With enough random samples drawn from the target distribution any value can be approximated by the probability distribution based on a specific set of constraints. An easy illustration of the property is the following relation:

$$\theta \sim N(\mu, \sigma) \tag{14}$$

In this relation we have a target distribution, $N(\mu, \sigma)$, which is a normal distribution and a constraint μ, which is the mean. With Monte Carlo a probability distribution will be created, based on a lot of random samples, that in time will give an approximation of θ. In this case the probability distribution will be the same as the normal distribution with $\theta \approx \mu$. [39, 40]

A Markov Chain generates a sequence, or chain, of variables where the current variable is based upon the prior variable and a variance. Putting those two together we get the Markov Chain Monte Carlo (MCMC) in which samples are drawn from a target distribution which depends on the prior value. To expand on the previous example, the relation will become:

$$\theta_t \sim N(\theta_{t-1}, \sigma) \tag{15}$$

The current iteration of θ is based on the normal distribution where the mean is equal to that of the previous iteration of θ. This creates a so called random walk around the parameter space. The chain will not converge. However, putting a restraint on this chain, for instance an acceptance criterion, would cause the chain to converge towards the approximation of a parameter. This is where Metropolis-Hastings comes in. [39, 40]

Metropolis-Hastings Metropolis-Hastings uses a accept-reject type of adjustment to let the Markov chain converge towards a stationary distribution approximating parameter θ. First it is good to state that we would like to draw the samples from a target distribution $p(\theta)$ but only know it is proportional to $g(\theta)$. Furthermore, the proposal distribution $q(\theta_{i-1}|\theta^*)$ is initially a normal distribution, but eventually q will switch to an adaptive proposal distribution based on the knowledge gathered about the distribution of g. Metropolis-Hastings follows the following steps:

1. Select the initial value θ_0
2. for $i = 1, ..., m$ repeat:
   (a) Draw candidate θ^* from a proposal distribution: $q(\theta^*|\theta_{i-1})$
   (b) Compute the acceptance ratio:
   $$\alpha = \frac{g(\theta^*)q(\theta_{i-1}|\theta^*)}{g(\theta_{i-1})q(\theta^*|\theta_{i-1})} \tag{16}$$
   (c) If $\alpha \geq 1$ accept θ^* and set $\theta_i = \theta^*$
   If $0 < \alpha < 1$ accept θ^* and set $\theta_i = \theta^*$ with probability α or
   reject θ^* and set $\theta_i = \theta_{i-1}$ with probability $1 - \alpha$

The eventual acceptance of a stationary chain and therefore a good approximation of the parameter, will depend on the statistics of the first half of the chain in comparison with the second half of the chain. If these overlap, stationarity has been reached. One important note is that the first 10% of the chain will not be taken into account when checking these statistics to limit the effect the initial choice has on the outcome. The elimination of the first, in this case, 10% is called the burn in period. Using these steps for m number of repeats will eventually result in an approximation for parameter θ. [39, 41]

Application in parameter estimation In this method, the Metropolis-Hastings algorithm determines the most likely parameter values $\mathbf{x}$, making up the modeled EEG power spectrum $P(\mathbf{x})$, that give rise to the experimental power spectrum P^{exp}. Specifically, it evaluates the posterior distribution of the parameters $P(\mathbf{x}|P^{exp})$ at a single point in $\mathbf{x}$-space. The posterior distribution is maximal when the model generates an optimal fit to the data.

The quality of the fit, $\chi^2(\mathbf{x})$, will be determined by a weighted squared fractional difference between $P(\mathbf{x})$ and p^{exp} given in the formula

$$\chi^2(\mathbf{x}) = \sum_j W_j(\frac{P_j(\mathbf{x}) - P_j^{exp}}{P_j^{exp}})^2 \tag{17}$$

j stands for the frequency components of the fast Fourier transform (FFT) of the experimental data and W is the weight, which ensures that every frequency from 1 till 45 Hz is weighed equally. The weight is defined as $W_j \propto f_j^{-1}$

The quality of fit is minimized when the best fit has been reached. To link the quality of fit to the posterior distribution, they defined the likelihood function

$$L(\mathbf{x}) = exp[\frac{-\chi^2(\mathbf{x})}{2}] \tag{18}$$

and set the posterior distribution proportional to the likelihood function

$$p(\mathbf{x}|p^{exp}) \propto L(\mathbf{x}) \tag{19}$$

The likelihood function is maximized when $\chi^2(\mathbf{x})$ is minimized, satisfying that $p(\mathbf{x}|P^{exp})$ is maximal at the most likely parameter values. One constraint to consider is that unphysiological parameter values will not be accepted.

3. Methods

3.1. Data acquisition and epoch selection

We acquired data from the clinical neurophysiology group of the University of Twente. These data were originally collected in Ruijter et al. [5]. Between July 2010 and September 2014, they collected EEG recordings of comatose patients admitted to the intensive care unit (ICU) after cardiac arrest, from two university hospitals in the Netherlands. Out of all the EEG recordings in their study they identified 47 patients with GPDs by means of a detection algorithm [42]. We performed an additional visual inspection and included 45 out of the 47 patients in our study. The two patients we excluded showed spike-wave discharges. We divided the 45 patients, by means of visual analysis, into patients with GPDs on a continuous background and patients with GPDs on a suppressed background. We also included 50 EEG recordings from healthy subjects showing a dominant occipital alpha rhythm, acquired from the clinical neurophysiology group of the university of Twente. These recordings were used as a control group for the parameter estimation.

3.1.1. EEG recordings

The EEG recordings were started as soon as possible within 24 hours after a patients' admission to the ICU. They continued until the patients were awake or the decision was made to withdraw treatment, with a maximum of 5 days. Twenty-one silver/silver chloride cup electrodes were placed on the scalp according to the international 10–20 system and quantitative EEG analysis was performed offline. The same setup was used for the control group.

3.1.2. Selection of EEG epochs

A five minute epoch was selected per EEG recording, for both comatose patients and healthy subjects. The five minute epochs of the comatose patients were already preselected in the study of Ruijter et al. [5]. They selected 5 minute epochs in the hour corresponding to the onset of the GPDs and subjected them to a computer algorithm used in a previous quantitative EEG study, to only select epochs free of artifacts [43]. The five minute epochs in the EEG recordings of healthy subjects were selected out of a longer EEG recording of up to one hour. We selected these epochs based on a visual inspection for a dominant occipital alpha rhythm and with the least amount of artefacts.

3.2. Data analysis

EEG analysis, source reconstruction and accompanying statistical analysis, and parameter estimation were performed with MATLAB(MathWorks Inc.; version r2022b) [44]. Fieldtrip toolbox(Donders Institute; version 20230118) and OpenMEEG(INRIA Sophia Antipolis; version 2.4.1) were used for source reconstruction and leadfield generation [21, 45, 46]. The Braintrak toolbox (BrainDynamics USYD; version Apr 18,2018) was

used for parameter estimation [37]. Statistical analysis of parameter estimates was performed with SPSS(IBM; version 28.0.1.0).

3.3. Source reconstruction

We performed source reconstruction on the EEG recordings of GPD patients using our own constructed pipeline based on the functions of the Fieldtrip toolbox [21]. Source reconstruction consists of three parts: the forward solution including anatomical information, EEG preprocessing, and the inverse solution (figure 1). All three parts are explained in the respective sections below.

3.3.1. Forward solution

We used the MNI (Montreal Neurological Institute) ICBM 2009c symmetric MRI template [47, 48, 49] as input to our volume conduction model, as there were no MRIs available for any of the patients. We segmented the following tissues from the MRI: brain, skull, and scalp, and constructed a 3-layer Boundary Element Method (BEM) volume conduction model, also known as a head model, using OpenMEEG [45, 46]. The conductivity of the brain, skull and scalp is set to 0.3300, 0.0042 and 0.3300 S/m respectively. The BEM head model consists of a mesh, or boundary, for each tissue and describes the current flow through the tissues. The electrode positions were based upon the standard 10-20 electrode template of Fieldtrip and we adjusted the labels to fit those in the EEG recordings. No patient specific electrode positions were used because they were not recorded. To complete the forward solution, we constructed a source space consisting of approximately 4500 source points equally distributed inside the brain.

3.3.2. EEG preprocessing

We split the EEG epochs into 10 second trials and removed the electrically silent electrodes A1 and A2 from the data. Additionally, if a single electrode per EEG was silent or experienced high power line interference, we removed the electrode from the data as well. We removed data from one electrode in 7 of the 45 comatose EEG recordings.

Afterwards, we subjected the 10 second trials to a jump, muscle and EOG artifact rejection algorithm in Fieldtrip [21]. This algorithm uses the averaged z-transform over all the channels to identify the above mentioned artifacts. We visually analyzed these z-transforms and, by means of a threshold, rejected the trials that exceeded this threshold.

Lastly, we filtered the EEG recordings in the interval 1Hz to 30Hz with a 2nd-order Butterworth filter and avoided phase distortion by using filtfilt. If needed, we changed the EEG montage to an average montage to create the correct input for the source analysis algorithm.

3.3.3. Inverse solution

We used eLORETA for the inverse solution. An in depth explanation of eLORETA can be found in section 2.2. After performing the inverse solution for all subjects, we normalized the solution per subject relative to the maximum power and created a mean source reconstruction plot per subject group. We considered every point in the source space with a power of more than 0.8 times the maximum power to be part of the same source.

3.3.4. Statistical analysis

To test for a difference in (peak) source location between the two GPD groups, we applied a permutation test [50]. We used the location parameters (i.e. x, y, z, coordinate) of the maximum power per subject as response values and the distance in mean of the response values between the groups as test statistic. We performed 10^4 random shifts to obtain a null distribution. The p-value was calculated by determining its position in this distribution. A p-value of ≤ 0.05 was considered statistically significant.

3.4. Parameter estimation

We performed parameter estimation on the EEG recordings of both GPD groups and healthy subjects using the model and method of Abeysuriya and Robinson [36, 37]. In this section, we provide a brief overview of both model and method. An extensive explanation of both model and method can be found in section 2.3.

Due to few global instabilities at low frequencies the model, as described in section 2.3, can be reduced to a three-dimensional representation: X representing the cortical loop, Y representing the corticothalamic loop, and Z representing the intrathalamic loop. Together, they capture the membrane potential and firing rate of the different loops (figure 3). This is the representation used in this thesis.

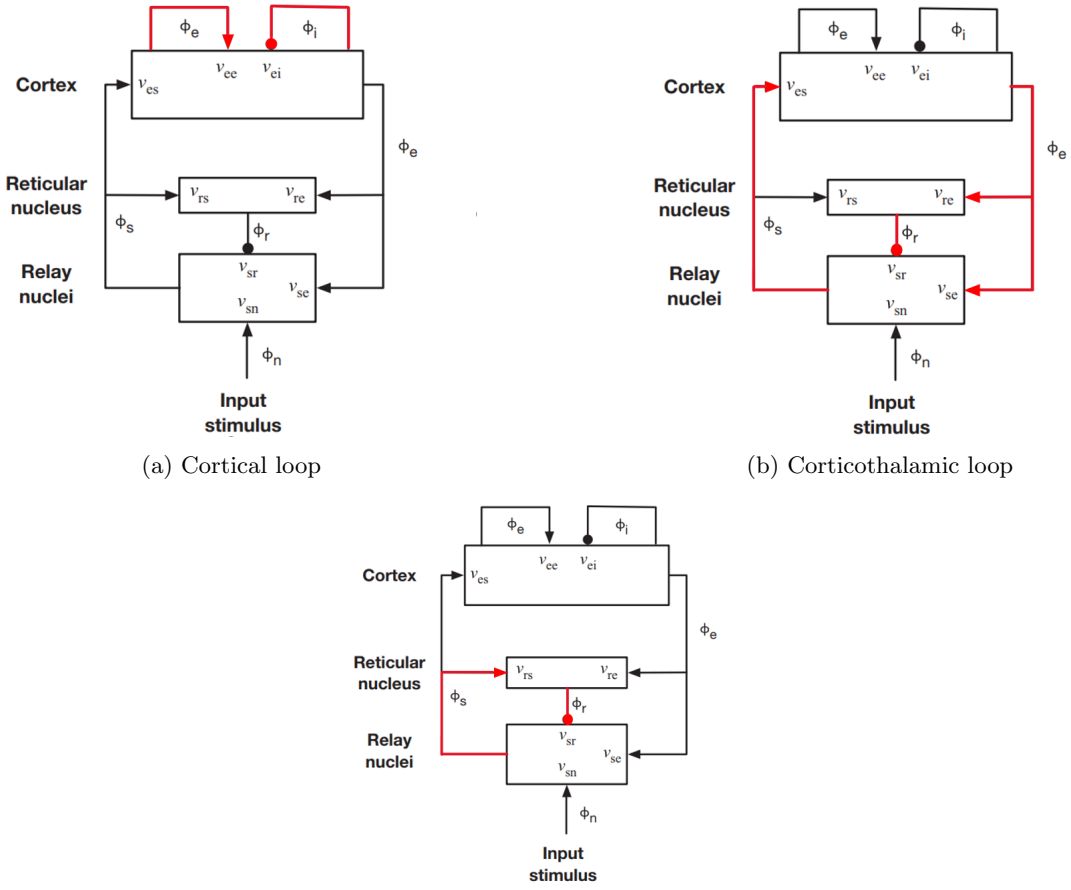

(a) Cortical loop

(b) Corticothalamic loop

(c) Intrathalamic loop

Figure 3: Schematic overview of the three different loops present in the corticothalamic meanfield model. From top left to bottom right: the cortical loop, corticothalamic loop and intrathalamic loop.

These loops can be mathematically described as:

$$X = \frac{G_{ee}}{1 - G_{ei}} \tag{20}$$

$$Y = \frac{G_{ese} + G_{esre}}{(1 - G_{srs})(1 - G_{ei})} \tag{21}$$

$$Z = -G_{srs} \frac{\alpha\beta}{(\alpha + \beta)^2} \tag{22}$$

Subsequently, we used Metropolis-Hastings to fit the following parameters: X, Y, Z, α, β, and $t0$ which is the delay in the corticothalamic loop.

3.4.1. EEG preprocessing

The method for parameter estimation is based on an experimental power density. To achieve the most accurate fit for the parameter estimation, as much of the original signal needs to be retained. We submitted the EEG recordings to as little preprocessing as possible. EEGs were only filtered with a 0.5Hz high pass filter, using a 2nd-order Butterworth and filtfilt to avoid phase distortion to remove the offset and drift. For the experimental power density, we used pwelch with a window of 5 seconds and 50% overlap between the windows.

3.4.2. Statistical analysis

To test the differences in the fitted parameters between the three groups, we applied Kruskall-Wallis because we could not guarantee a normal distribution. If the Kruskal-Wallis test was significant, we applied the Mann-Whitney U test to test between-group differences. All statistical testing was two-tailed and p-values ≤ 0.05, after a Bonferroni correction, were considered statistically significant.

4. Results

4.1. Patient groups

Out of the 45 patients included in this study, we visually identified 26 patients with GPDs on a continuous background(GPDcont) and 19 with GPDs on a suppressed background(GPDsup). Figure 4 shows typical examples of GPDs on a continuous background and GPDs on a suppressed background.

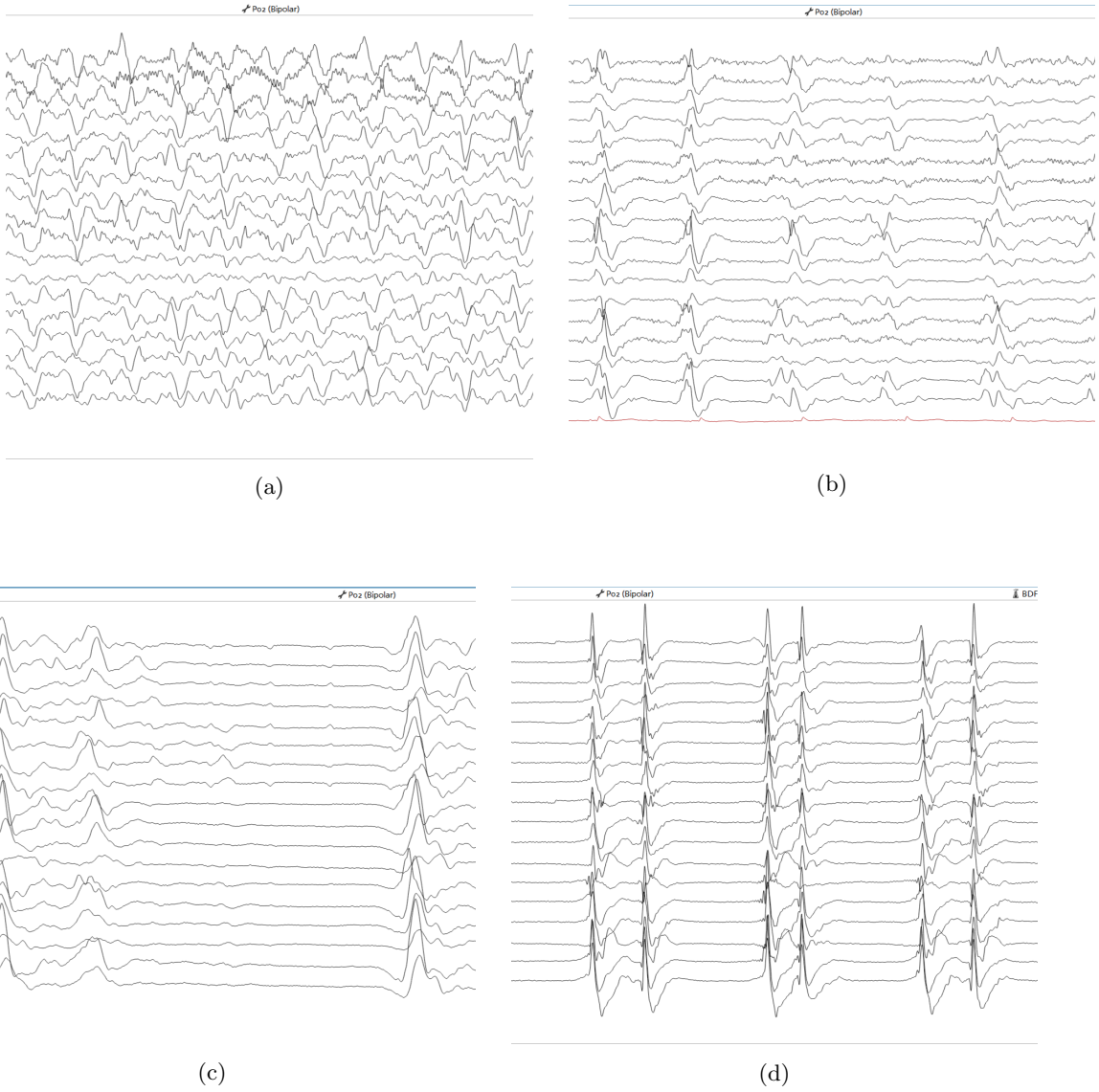

Figure 4: Typical examples of GPDs on a continuous background (a,b) and of GPDs on a suppressed background (c,d)

4.2. Source reconstruction

Source reconstruction revealed that the maximum power for both GPD groups was predominantly found in the subcortical regions. This was the case for 15/26 patients with GPDcont and 10/19 patients with GPDsup. Subcortical regions included the anterior cingulate gyrus, corpus callosum, thalamus, hypothalamus, and amygdala. Other patients showed maximum power in the occipital lobe (2 patients with GPDcont and 1 patient with GPDsup), frontal lobe (3 patients with GPDcont and 1 patient with GPDsup) medial-orbitofrontal(1 patients with GPDcont and 3 patient with GPDsup) parietal lobe (2 patients with GPDcont and 2 patient with GPDsup), and cerebellum (3 patients with GPDcont and 2 patient with GPDsup).

Averaging over all subjects per subject group and including only points in the source space with a value of $\geq 0.8 * max\_power$, shows a maximum power in only the subcortical regions (figure 5). The scatterplot in figure 6 shows all the points of maximum power per group plotted at their respective brain coordinates. The scatterplot shows no distinct groups of points, illustrating the lack of signifcant difference between between the average location with maximum power of both groups ($p = 0.58$).

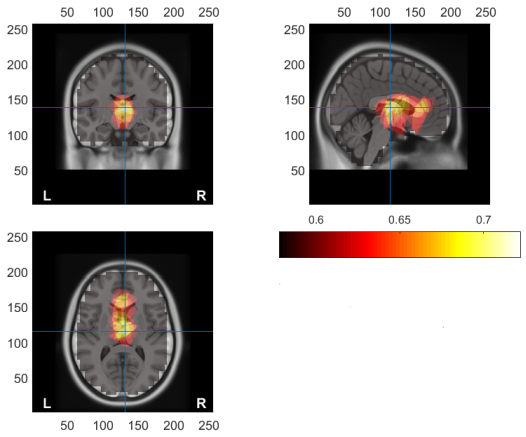

(a) GPDs on a continuous background

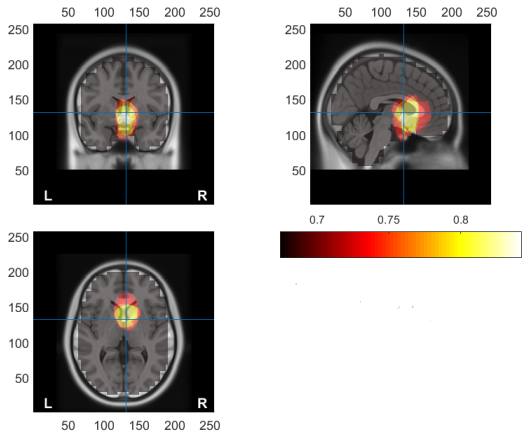

(b) GPDs on a suppressed background

Figure 5: Average of all subjects per subject group, with a constraint of showing only points in the source space with a value of $\geq 0.8 * max\_power$. Both figures show a maximum power in the subcortical regions including: anterior cingulate gyrus, corpus callosum, thalamus, hypothalamus and amygdala. There is no significant difference in average location of the maximum power between the groups.

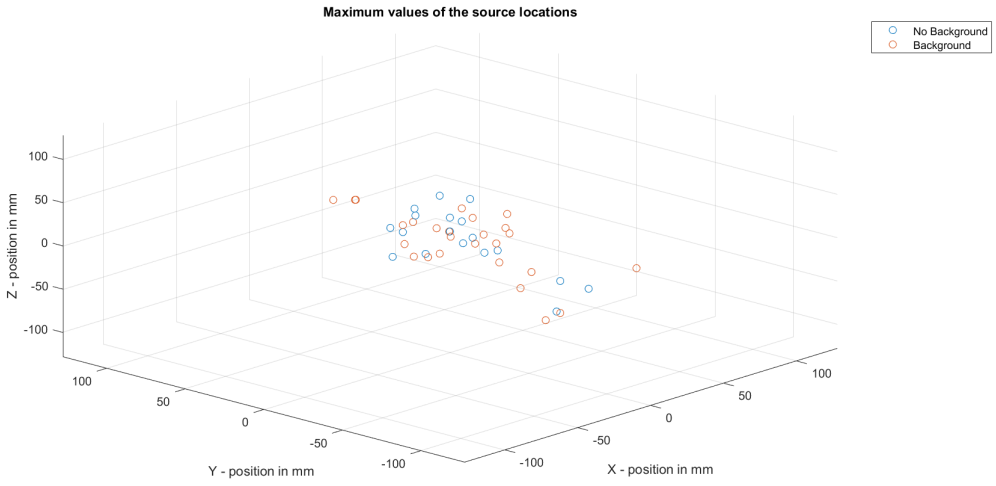

Figure 6: Scatterplot of all coordinates corresponding to the maximum source power for all subjects in both groups. Blue points represent GPDsup and the red points represent the GPDcont. There is no significant difference between both GPD groups.

4.3. Parameter estimation

Parameter estimation revealed significant differences between both GPD groups compared to healthy controls in the median of the cortical loop (X), corticothalamic loop (Y), corticothalamic delay *(t0)*, and rise rate (β). The intrathalamic loop Z showed only a significant difference between GPDsup and healthy controls (HC) and α showed a significant difference between GPDcont and GPDsup, and GPDcont and HC (figure 7).

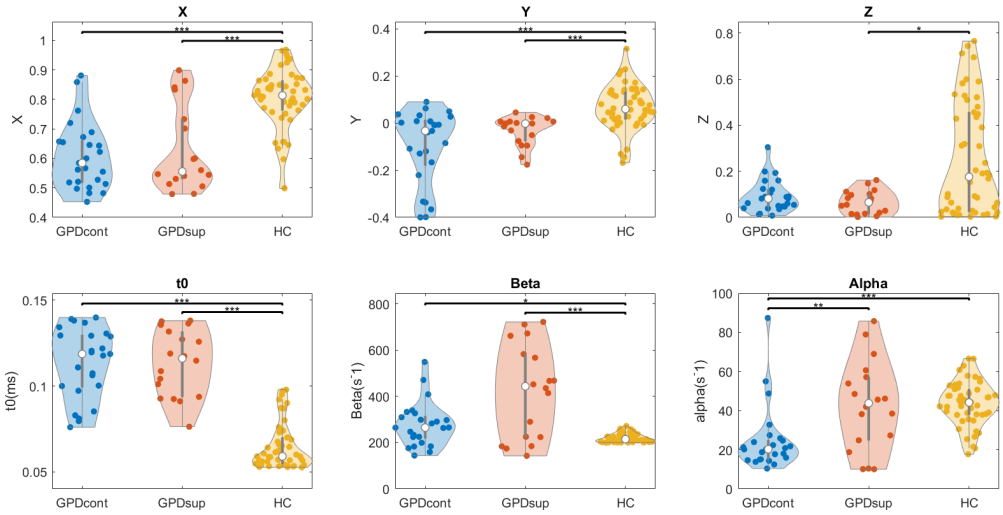

Figure 7: Violin plots of all the fitted variables of the corticothalamic model [37]. There were significant differences in median of both GPD groups compared to healthy controls in: X, Y, $t0$, and β. While Z showed only a significant difference between GPDsup and healthy controls (HC) and α showed a significant difference between GPDcont and GPDsup, and GPDcont and HC.*,** and *** signify an increase in significance. They are associated with $p \leq 0.05$ $p \leq 1e-2$, $p \leq 1e-3$ respectively.

Patients with GPDcont and GPDsup had significantly lower X-values than healthy subjects ($U(2) = -33.56, p < 0.001$ and $U(2) = -29.23, p < 0.001$, respectively). There was no significant difference in X-value in between the GPD groups ($U(2) = -4.32, p > 0.05$). For the corticothalamic loop, the Y-values of both GPD groups, lay closer to zero or are negative compared to mostly positive values in the HC ($U(2) = -32.74, p < 0.001$ and $U(2) = -30.27, p < 0.001$, for GPDcont and GPDsup respectively). Again, there is no significant difference between the two GPD groups ($U(2) = -2.46, p > 0.05$). The same holds for the corticothalamic delay, only $t0$ is significantly larger in both GPD groups, compared to HC ($U(2) = 44.00, p < 0.001$ and $U(2) = 43.87, p < 0.001$, for GPDcont and GPDsup respectively), while between the GPD groups there is no significant difference in $t0$ ($U(2) = 0.12, p > 0.05$).

The rise rate (β) is significantly higher in median for both GPD groups than the HC, however it is not as profound as in previous variables ($U(2) = 17.02, p = 0.03$ and $U(2) = 25.86, p = 0.001$, for GPDcont and GPDsup respectively). There is no significant difference in rise rate between the two GPD groups ($U(2) = -8.84, p > 0.05$). The decay rate is significantly lower in patients with GPDcont compared to patients with GPDsup ($U(2) = -27.07, p = 0.04$) and compared to HC ($U(2) = -31.92, p < 0.001$). There was no significant difference in decay rate between patients with GPDsup and HC ($U(2) = -4.85, p > 0.05$).

The intrathalamic loop variable, Z, was significantly higher in between the HC and patients with GPDsup ($U(2) = -18.75, p = 0.034$). No significant difference in Z-value had been found between patients with GPDcont and HC($U(2) = -11.20, p > 0.05$), and in between both GPD groups($U(2) = 7.55, p > 0.05$). HC displayed a greater variance of Z-values with an increase in probability density at lower values, while GPD groups displayed a low variance around low z-values.

5. Discussion

The mortality rate of comatose patients with postanoxic encephalopathy after an out-of-hospital cardiac arrest is 50%. Generalized periodic discharges (GPDs) are an EEG pattern that occurs in 20% of these patients and is associated with a poor outcome [3, 7, 18, 51]. However, a recent study by Ruijter et al. [5] differentiated GPDs into two types. GPDs on a suppressed background associated with a poor outcome (CPC 3-5), and GPDs on a continuous background associated with a good outcome (CPC 1-2). Why this difference in outcome between the two types of GPDs occurs remains unclear. Identification of the anatomical source and underlying pathophysiology of both types would provide a greater understanding of why this difference occurs and would further expand our understanding of the underlying pathophysiology of GPDs.

In this study, we applied source reconstruction, and parameter estimation on a corticothalamic meanfield model to both types of GPDs. We have found no significant differences in the anatomical source between the two types of GPDs. Parameter estimation revealed no significant differences between the two GPD groups, except for the decay rate. However, we did find a significant difference in both the cortical and corticothalamic loop variables between the GPD groups and healthy controls. This suggests the involvement of both the cortex and the thalamus in the generation of GPDs.

Based only on significant differences between the GPD groups, our results suggest that the difference in prognosis between the two GPD groups could be clarified by a significant difference in decay rate alone. Why we believe this is not the case, is later explained in this section. We hypothesize that the continuous background itself could cause the difference in prognosis. Ruijter et al. [5] discovered that patients, who recovered with a CPC of 1-2 (considered a good outcome), had a continuous background prior to onset of GPDs. A continuous EEG, diffusely slowed or normal, on its own is associated with a good outcome, while GPDs on their own are associated with a poor outcome [51, 52]. The earlier onset of a continuous background could indicate a sufficient recovery of the brain. The onset of GPDs in a later stage would therefore have less influence on the eventual outcome.

A significantly lower and even negative values of the corticothalamic loop variable Y, a significant increase in the corticothalamic delay $t0$ and an anatomical source in the subcortical regions strongly suggests the involvement of the thalamus in the generation or spread of GPDs. Previous studies have shown that the thalamus is involved in the generation of EEG patterns similar to GPDs, specifically burst suppression and generalized rhythmic spike-wave discharges [53, 54]. Furthermore, in [3] they concluded, using source reconstruction, that the thalamus, hippocampus, and amygdala are the main drivers of GPDs. These reports strengthen our suggestion that the thalamus is involved in the generation or spread of GPDs.

The negative values of Y and the increase in $t0$ illustrate the underlying mechanisms of GPDs. A negative value for the corticothalamic loop, Y, compared to healthy controls could be explained by an increase in the inhibitory gain G_{esre} compared to the excitatory gain G_{ese}. A relative increase of G_{esre} means a relative increase in the excitation of the inhibitory reticular neurons compared to excitatory neurons. This is in contrast with previous research, which revealed that inhibitory reticular neurons are especially sensitive to hypoxia and that injury to these neurons results in an increased spontaneous and evoked firing rates among thalamocortical neurons [55]. Further research is needed. The increase in total time delay for the corticothalamic loop, $t0$, could be explained by an overall decrease in the number of synapses between the cortex and thalamus due to ischaemia.

The significant decrease in the cortical loop, X, between both GPD groups and healthy controls suggests the involvement of the cortex in the generation or spread of GPDs as well. The significant decrease could be explained by an increase of G_{ei} compared to G_{ee}. An increase in the inhibitory gain can only be explained by an increase in excitation of the inhibitory neurons. While an increase in the number of synapses is not likely due to the ischaemia, an increase in strength of the soma response S_{ab} could explain the increase in inhibitory gain. This is also in line with the findings in [56], who concluded that the loss of excitation of cortical interneurons due to selective ischemia-induced synaptic failure leads to disinhibition of pyramidal neurons and therefore to higher excitation of interneurons.

The parameter variable of the intrathalamic loop Z revealed only a significant difference between the healthy controls and patients with GPDs on a suppressed background. Visually, there is a difference between the GPD groups and healthy controls, in which healthy controls show a greater variance in the value Z. To understand the Z value we also have to take into account the variables α, the decay rate, and β, the rise rate. The decrease in variance in Z in the GPD groups is most likely due to a decrease in G_{srs}, which in turn is caused by a decrease in the number of synapses due to ischaemia. This assumption is reinforced by the fact that a large variance in α and β in the patient group with GPDs on a suppressed background still results in a significantly low Z value compared to healthy controls. In other words, the influence of α and β is less than that of G_{srs} on the Z value, in the case of the GPD groups. The high variance in α and β in the patient group with GPDs on a suppressed background could be explained by the variance in morphology of the GPDs, which exhibit different rise and decay rates (figure 4).

We did not expect the Z in the healthy controls to have a greater variance than the GPD groups. G_{srs}, the number of synapses, and the strength of the soma potential should not differ much in healthy controls. Z is expected to be significantly different from both GPD groups, yet due to the high variance this is not the case. We do not know why the high variance occurs in Z. We were also not able to determine why the α value has a significantly lower median in the patient group with GPDs on a continuous background compared to the other groups. It could be pathological, yet if it was pathological it should have been more present in the other GPD group. It could also be due to the morphology of the EEG in which the continuous background interferes with GPDs causing a decrease in decay rate. However, further research is needed.

5.1. Limitations

This study has limitations. First, a larger sample size of both types of GPDs would give a more clear result in both source reconstruction and parameter estimation. It would provide a higher resolution for the source location and could resolve the unanswered questions around the Z and α values. The resolution of the source reconstruction would also benefit from adding patient specific: MRI data, conductivity parameters, and electrode positions. Second, our data consisted of low-density EEG recording, which limit the accuracy of the source reconstruction as well. The accuracy was specific enough to identify the involvement of the subcortical region in the onset of GPDs, but insufficient enough to identify specific brain structures by means

of an anatomical atlas. Third, we classified the types of GPDs by means of visual analysis. It would have been an improvement if we had automated the distinction between GPDs on a continuous or suppressed background by using the background continuity parameter developed by Ruijter et al. [5]. This parameter gives a ratio between 0 and 1 based on the amount of time the EEG is $\geq 10\mu V$, in which a value of 0.9 or higher indicates a continuous background. This quantitative method is a more robust way of classifying the GPDs into the two different types. Last, we were unable to fully explain the influence of the intrathalamic loop on the generation of GPDs, because we were unable to clarify the variance of the Z value of healthy controls and the significantly lower α value of the patient group with GPDs on a continuous background.

6. Conclusion and Recommendations

We conclude that a difference in prognosis between both types of GPDs cannot be explained by a difference in anatomical source or pathophysiological variables of the corticothalamic meanfield model, despite the significant difference in the decay rate. Instead we hypothesize that the difference in prognosis could be attributed to the difference in background, continuous or suppressed. Further, we found a strong suggestion that both the cortical and corticothalamic loop are involved in the spread or generation of GPDs. In both cases the gain of the inhibiting neurons increased relative to the gain of the excitatory neurons. Although still a lot of research has to be done to fully understand the underlying pathophysiological mechanisms of GPDs, our research has added to our general understanding of generalized periodic discharges.

6.1. Future recommendations

We highly recommend to further investigate the underlying pathophysiology of GPDs as there is still a lot of research to be done to fully understand these underlying mechanisms. For instance, although we found strong evidence of the involvement of the thalamus in the spread or generation of GPDs, we do not know if the thalamus is the actual generator or just a gateway for these GPDs. Furthermore, we hypothesize that our results only reflect the anatomical source and pathophysiology of the GPDs itself and do not reflect the anatomical source and pathophysiology of the background they occur on. We highly recommend to investigate the effect of the continuous background on the prognosis of patients with GPDs this background. For instance, by separately investigating the GPDs and the continuous background using source reconstruction and parameter estimation. Lastly, our results only reflect one moment in time and do not show the time evolution of GPDs. We highly recommend to investigate the time evolution of GPDs, as this could reveal more about the onset and pathophysiological evolution of GPDs.

References

[1] J. Hofmeijer and M. E.W. Hemels. Recovery after cardiac arrest: the brain is the heart of the matter. *Netherlands Heart Journal*, 26:484–485, 2018.

[2] J. Horn, C.W.E. Hoedemaekers, J. Hofmeijer, L.S.D. Jewbali, J.H.T.M. Koelman, and W. de Ruijter. Prognose van postanoxisch coma, 2 2019.

[3] Pia De Stefano, Margherita Carboni, Deborah Pugin, Margitta Seeck, and Serge Vulliémoz. Brain networks involved in generalized periodic discharges (gpd) in post-anoxic-ischemic encephalopathy. *Resuscitation*, 155:143–151, 10 2020.

[4] Andrea O. Rossetti, Mauro Oddo, Giancarlo Logroscino, and Peter W. Kaplan. Prognostication after cardiac arrest and hypothermia: A prospective study. *Annals of Neurology*, pages NA–NA, 2010.

[5] Barry J. Ruijter, Michel J.A.M. Van Putten, and Jeannette Hofmeijer. Generalized epileptiform discharges in postanoxic encephalopathy: Quantitative characterization in relation to outcome. *Epilepsia*, 56:1845–1854, 11 2015.

[6] Lawrence J. Hirsch, Michael W.K. Fong, Markus Leitinger, Suzette M. LaRoche, Sandor Beniczky, Nicholas S. Abend, Jong Woo Lee, Courtney J. Wusthoff, Cecil D. Hahn, M. Brandon Westover, Elizabeth E. Gerard, Susan T. Herman, Hiba Arif Haider, Gamaleldin Osman, Andres Rodriguez-Ruiz, Carolina B. Maciel, Emily J. Gilmore, Andres Fernandez, Eric S. Rosenthal, Jan Claassen, Aatif M. Husain, Ji Yeoun Yoo, Elson L. So, Peter W. Kaplan, Marc R. Nuwer, Michel van Putten, Raoul Sutter, Frank W. Drislane, Eugen Trinka, and Nicolas Gaspard. American clinical neurophysiology society's standardized critical care eeg terminology: 2021 version. *Journal of Clinical Neurophysiology*, 38:1–29, 1 2021.

[7] Michel J.A.M. van Putten and Jeannette Hofmeijer. Generalized periodic discharges: Pathophysiology and clinical considerations. *Epilepsy and Behavior*, 49:228–233, 8 2015.

[8] U.S. Department of Health and Human Services. Encephalopathy. `https://www.ninds.nih.gov/health-information/disorders/encephalopathy`, 2023. [Online; accessed 9-May-2023].

[9] Sjoukje Nutma, Joost le Feber, and Jeannette Hofmeijer. Neuroprotective treatment of postanoxic encephalopathy: A review of clinical evidence. *Frontiers in Neurology*, 12, 2 2021.

[10] Katharina M. Busl and David M. Greer. Hypoxic-ischemic brain injury: Pathophysiology, neuropathology and mechanisms. *NeuroRehabilitation*, 26:5–13, 1 2010.

[11] Timothy H. Murphy and Dale Corbett. Plasticity during stroke recovery: from synapse to behaviour. *Nature Reviews Neuroscience*, 10:861–872, 12 2009.

[12] G Buunk. Cerebral blood flow after cardiac arrest. *The Netherlands Journal of Medicine*, 57:106–112, 9 2000.

[13] Miao-Kun Sun, Hui Xu, and Daniel L. Alkon. Pharmacological protection of synaptic function, spatial learning, and memory from transient hypoxia in rats. *Journal of Pharmacology and Experimental Therapeutics*, 300:408–416, 2 2002.

[14] Jeannette Hofmeijer and Michel J.A.M. van Putten. Ischemic cerebral damage. *Stroke*, 43:607–615, 2 2012.

[15] Barry J. Ruijter, Marleen C. Tjepkema-Cloostermans, Selma C. Tromp, Walter M. van den Bergh, Norbert A. Foudraine, Francois H. M. Kornips, Gea Drost, Erik Scholten, Frank H. Bosch, Albertus Beishuizen, Michel J. A. M. van Putten, and Jeannette Hofmeijer. Early electroencephalography for outcome prediction of postanoxic coma: A prospective cohort study. *Annals of Neurology*, 86:203–214, 8 2019.

[16] Koen Dijkstra, Jeannette Hofmeijer, Stephan A. van Gils, and Michel J.A.M. van Putten. A biophysical model for cytotoxic cell swelling. *The Journal of Neuroscience*, 36:11881–11890, 11 2016.

[17] Ming-Chi Lai and San-Nan Yang. Perinatal hypoxic-ischemic encephalopathy. *Journal of Biomedicine and Biotechnology*, 2011:1–6, 2011.

[18] Claire Thornton and Henrik Hagberg. Role of mitochondria in apoptotic and necroptotic cell death in the developing brain. *Clinica Chimica Acta*, 451:35–38, 12 2015.

[19] A Ames, R L Wright, M Kowada, J M Thurston, and G Majno. Cerebral ischemia. ii. the no-reflow phenomenon. *The American journal of pathology*, 52:437–53, 2 1968.

[20] Rey Ramírez. Source localization. *Scholarpedia*, 3:1733, 2008.

[21] Robert Oostenveld, Pascal Fries, Eric Maris, and Jan-Mathijs Schoffelen. Fieldtrip: Open source software for advanced analysis of meg, eeg, and invasive electrophysiological data. *Computational Intelligence and Neuroscience*, 2011:1–9, 2011.

[22] Christoph M. Michel and Denis Brunet. Eeg source imaging: A practical review of the analysis steps. *Frontiers in Neurology*, 10, 2019.

[23] Roberto D. Pascual-Marqui. Discrete, 3D distributed, linear imaging methods of electric neuronal activity. Part 1: exact, zero error localization. `http://arxiv.org/pdf/0710.3341`, 10 2007.

[24] Munsif Ali Jatoi, Nidal Kamel, Aamir Saeed Malik, and Ibrahima Faye. Eeg based brain source localization comparison of sloreta and eloreta. *Australasian Physical and Engineering Sciences in Medicine*, 37:713–721, 12 2014.

[25] Olaf Hauk. Keep it simple: A case for using classical minimum norm estimation in the analysis of eeg and meg data. *NeuroImage*, 21:1612–1621, 4 2004.

[26] Roberta Grech, Tracey Cassar, Joseph Muscat, Kenneth P. Camilleri, Simon G. Fabri, Michalis Zervakis, Petros Xanthopoulos, Vangelis Sakkalis, and Bart Vanrumste. Review on solving the inverse problem in eeg source analysis. *Journal of NeuroEngineering and Rehabilitation*, 5, 2008.

[27] Shiva Asadzadeh, Tohid Yousefi Rezaii, Soosan Beheshti, Azra Delpak, and Saeed Meshgini. A systematic review of eeg source localization techniques and their applications on diagnosis of brain abnormalities. *Journal of Neuroscience Methods*, 339, 6 2020.

[28] Margherita Carboni, Denis Brunet, Martin Seeber, Christoph M. Michel, Serge Vulliemoz, and Bernd J. Vorderwülbecke. Linear distributed inverse solutions for interictal eeg source localisation. *Clinical Neurophysiology*, 133:58–67, 1 2022.

[29] Martin Seeber, Lucia-Manuela Cantonas, Mauritius Hoevels, Thibaut Sesia, Veerle Visser-Vandewalle, and Christoph M. Michel. Subcortical electrophysiological activity is detectable with high-density eeg source imaging. *Nature Communications*, 10:753, 2 2019.

[30] Pavitra Krishnaswamy, Gabriel Obregon-Henao, Jyrki Ahveninen, Sheraz Khan, Behtash Babadi, Juan Eugenio Iglesias, Matti S. Hämäläinen, and Patrick L. Purdon. Sparsity enables estimation of both subcortical and cortical activity from meg and eeg. *Proceedings of the National Academy of Sciences*, 114, 11 2017.

[31] Maria Carla Piastra, Andreas Nüßing, Johannes Vorwerk, Maureen Clerc, Christian Engwer, and Carsten H. Wolters. A comprehensive study on electroencephalography and magnetoencephalography sensitivity to cortical and subcortical sources. *Human Brain Mapping*, 42:978–992, 3 2021.

[32] Pieter van Mierlo, Gregor Strobbe, Vincent Keereman, Gwénael Birot, Stefanie Gadeyne, Markus Gschwind, Evelien Carrette, Alfred Meurs, Dirk Van Roost, Kristl Vonck, Margitta Seeck, Serge Vulliémoz, and Paul Boon. Automated long-term eeg analysis to localize the epileptogenic zone. *Epilepsia Open*, 2:322–333, 9 2017.

[33] Ana Coito, Silke Biethahn, Janina Tepperberg, Margherita Carboni, Ulrich Roelcke, Margitta Seeck, Pieter Mierlo, Markus Gschwind, and Serge Vulliemoz. Interictal epileptogenic zone localization in patients with focal epilepsy using electric source imaging and directed functional connectivity from low-density ¡scp¿eeg¡/scp¿. *Epilepsia Open*, 4:281–292, 6 2019.

[34] Willeke Staljanssens, Gregor Strobbe, Roel Van Holen, Vincent Keereman, Stefanie Gadeyne, Evelien Carrette, Alfred Meurs, Francesca Pittau, Shahan Momjian, Margitta Seeck, Paul Boon, Stefaan Vandenberghe, Serge Vulliemoz, Kristl Vonck, and Pieter van Mierlo. Eeg source connectivity to localize the seizure onset zone in patients with drug resistant epilepsy. *NeuroImage: Clinical*, 16:689–698, 2017.

[35] Pieter van Mierlo, Gregor Strobbe, Vincent Keereman, Gwénael Birot, Stefanie Gadeyne, Markus Gschwind, Evelien Carrette, Alfred Meurs, Dirk Van Roost, Kristl Vonck, Margitta Seeck, Serge Vulliémoz, and Paul Boon. Automated long-term eeg analysis to localize the epileptogenic zone. *Epilepsia Open*, 2:322–333, 9 2017.

[36] R.G. Abeysuriya, C.J. Rennie, and P.A. Robinson. Physiologically based arousal state estimation and dynamics. *Journal of Neuroscience Methods*, 253:55–69, 9 2015.

[37] R. G. Abeysuriya and P. A. Robinson. Real-time automated eeg tracking of brain states using neural field theory. *Journal of Neuroscience Methods*, 258:28–45, 1 2016.

[38] S.J. van Albada, C.C. Kerr, A.K.I. Chiang, C.J. Rennie, and P.A. Robinson. Neurophysiological changes with age probed by inverse modeling of eeg spectra. *Clinical Neurophysiology*, 121:21–38, 1 2010.

[39] Kandethody M. Ramachandran and Chris P. Tsokos. Empirical methods, 2021.

[40] StataCorp LLC. Introduction to bayesian statistics, part 2: Mcmc and the metropolis–hastings algorithm, 2016.

[41] Matthew Heiner. Understanding metropolis-hastings algorithm, 2020.

[42] W. Deburchgraeve, P.J. Cherian, M. De Vos, R.M. Swarte, J.H. Blok, G.H. Visser, P. Govaert, and S. Van Huffel. Automated neonatal seizure detection mimicking a human observer reading eeg. *Clinical Neurophysiology*, 119:2447–2454, 11 2008.

[43] Marleen C Tjepkema-Cloostermans, Fokke B van Meulen, Gjerrit Meinsma, and Michel JAM van Putten. A cerebral recovery index (cri) for early prognosis in patients after cardiac arrest. *Critical Care*, 17:R252, 2013.

[44] The MathWorks Inc. Matlab version: 9.13.0 (r2022b), 2022.

[45] Alexandre Gramfort, Théodore Papadopoulo, Emmanuel Olivi, and Maureen Clerc. Openmeeg: opensource software for quasistatic bioelectromagnetics. *BioMedical Engineering OnLine*, 9:45, 2010.

[46] J. Kybic, M. Clerc, T. Abboud, O. Faugeras, R. Keriven, and T. Papadopoulo. A common formalism for the integral formulations of the forward eeg problem. *IEEE Transactions on Medical Imaging*, 24:12–28, 1 2005.

[47] VS Fonov, AC Evans, RC McKinstry, CR Almli, and DL Collins. Unbiased nonlinear average age-appropriate brain templates from birth to adulthood. *NeuroImage*, 47:S102, 7 2009.

[48] Vladimir Fonov, Alan C. Evans, Kelly Botteron, C. Robert Almli, Robert C. McKinstry, and D. Louis Collins. Unbiased average age-appropriate atlases for pediatric studies. *NeuroImage*, 54:313–327, 1 2011.

[49] D. Louis Collins, Alex P. Zijdenbos, Wim F. C. Baaré, and Alan C. Evans. Animal+insect: Improved cortical structure segmentation, 1999.

[50] Eric Maris and Robert Oostenveld. Nonparametric statistical testing of eeg- and meg-data. *Journal of Neuroscience Methods*, 164:177–190, 8 2007.

[51] A. O. Rossetti, G. Logroscino, L. Liaudet, C. Ruffieux, V. Ribordy, M. D. Schaller, P. A. Despland, and M. Oddo. Status epilepticus: An independent outcome predictor after cerebral anoxia. *Neurology*, 69:255–260, 7 2007.

[52] Marleen C. Tjepkema-Cloostermans, Jeannette Hofmeijer, Ronald J. Trof, Michiel J. Blans, Albertus Beishuizen, and Michel J. A. M. van Putten. Electroencephalogram predicts outcome in patients with postanoxic coma during mild therapeutic hypothermia*. *Critical Care Medicine*, 43:159–167, 1 2015.

[53] Natia Japaridze, Muthuraman Muthuraman, Christine Reinicke, Friederike Moeller, Abdul Rauf Anwar, Kidist Gebremariam Mideksa, Ronit Pressler, Günther Deuschl, Ulrich Stephani, and Michael Siniatchkin. Neuronal networks during burst suppression as revealed by source analysis. *PloS one*, 10:e0123807, 2015.

[54] J. Gotman, C. Grova, A. Bagshaw, E. Kobayashi, Y. Aghakhani, and F. Dubeau. Generalized epileptic discharges show thalamocortical activation and suspension of the default state of the brain. *Proceedings of the National Academy of Sciences*, 102:15236–15240, 10 2005.

[55] Michael Shoykhet, Daniel J. Simons, Henry Alexander, Christina Hosler, Patrick M. Kochanek, and Robert S. B. Clark. Thalamocortical dysfunction and thalamic injury after asphyxial cardiac arrest in developing rats. *The Journal of Neuroscience*, 32:4972–4981, 4 2012.

[56] Marleen C. Tjepkema-Cloostermans, Rikkert Hindriks, Jeannette Hofmeijer, and Michel J.A.M. van Putten. Generalized periodic discharges after acute cerebral ischemia: Reflection of selective synaptic failure? *Clinical Neurophysiology*, 125:255–262, 2 2014.